arXiv:1611.09483v1 [cond-mat.stat-mech] 29 Nov 2016

Graph's Topology and Free Energy of a Spin Model on the Graph

Jeong-Mo Choi,* Amy I. Gilson,† and Eugene I. Shakhnovich‡
Department of Chemistry and Chemical Biology, Harvard University, 12 Oxford Street, Cambridge, Massachusetts 02138, USA
(Dated: November 30, 2016)

In this work we show that there is a direct relationship between a graph's topology and the free energy of a spin system on the graph. We develop a method of separating topological and enthalpic contributions to the free energy, and find that considering the topology is sufficient to qualitatively compare the free energies of different graph systems at high temperature, even when the energetics are not fully known. This method was applied to the metal lattice system with defects, and we found that it partially explains why point defects are more stable than high-dimensional defects. Given the energetics, we can even quantitatively compare free energies of different graph structures via a closed form of linear graph contributions. The closed form is applied to predict the sequence space free energy of lattice proteins, which is a key factor determining the designability of a protein structure.

Over the last thirty years, graph theory has been applied to the study of various networks, including protein interaction networks, neural networks, and the World Wide Web [1–4]. Especially the interplay between network structure and dynamics has attracted considerable attention [5], while the equilibrium characteristics of networks, which may deepen our understanding of network phenomena, have not yet been studied thoroughly [6].

In this work, we will consider a spin model on a graph, which has a wide range of applications from gene expression on biochemical networks [7] to social network phenomena [8], and study an analytical relationship between a system's graph topology and its free energy. Such a relationship would be useful when discriminating between topologies based on their stability, and it could even provide the insight into graph dynamics, although we only consider systems with fixed graph topology here.

Consider a simple graph [9] of N nodes. The graph connectivity is described by the adjacency matrix A, whose element A_{ij} is 1 when there is a link between nodes i and j, and $A_{ij} = 0$ otherwise. Each node is in one of M possible spin states. The Hamiltonian, $\mathcal{H}$, is defined as the summation of energetic contributions over all links, each of whose energy is determined by the states of its two terminal nodes. Note that orphan nodes do not contribute energetically, by definition. Now, the Hamiltonian can be written formally as

$$\mathcal{H} = \frac{1}{2}\sum_{i,j}^{N,N} A_{ij}E_{s(i)s(j)}, \tag{1}$$

where E is the energy matrix and $s(i)$ is the state of node i. The high-temperature expansion of the partition function $Z(\beta) = \sum_{\{s\}} e^{-\beta\mathcal{H}}$ over all possible state configurations is

$$Z(\beta) = \sum_{\{s\}} 1 - \beta\sum_{\{s\}}\mathcal{H} + \frac{\beta^2}{2!}\sum_{\{s\}}\mathcal{H}^2 - \cdots. \tag{2}$$

In the higher-order terms, there are summations of various products of A and E elements. To systematically visualize those terms, we introduce a multigraph g (where multiple links between any pair of nodes are allowed) with no orphan nodes (see Fig. 1 for examples), and we use its nodes as dummy variables of the summations. For each multigraph g, we define two quantities $[g]$ and $E(g)$ as follows:

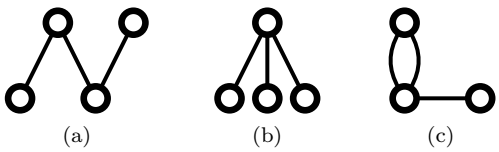

FIG. 1: Examples of 3-link multigraphs. a is a parent graph of c (*i.e.*, c is obtained by a node contraction operation on a), and b is also a parent graph of c, but there is no such relationship between a and b.

$$[g] = \sum_{\text{nodes}}\prod_{k=1}^{n(g)} A_{l_k}, \tag{3}$$

$$E(g) = M^{-n(\text{nodes})}\sum_{\text{nodes}}\prod_{k=1}^{n(g)} E_{l_k}, \tag{4}$$

where l_k indicates the link of index k, $n(g)$ is the number of links in graph g, and $n(\text{nodes})$ is the number of nodes in graph g. For example, for the graph shown in Fig. 1c,

$$\left[\;\right] = \sum_{ijk} A_{ij}A_{ij}A_{jk}, \tag{5}$$

$$E\left(\;\right) = M^{-3}\sum_{mnp} E_{mn}E_{mn}E_{np}. \tag{6}$$

Note that since A is a binary matrix, $[g]$ for a graph g with multiple links is equal to $[g_0]$ where g_0 is a simple graph constructed from g by converting all multiple links in g to single links. For example, equation 5 becomes

$$\left[\;\right] = \sum_{ijk} A_{ij}^2A_{jk} = \sum_{ijk} A_{ij}A_{jk} = \left[\;\right]. \tag{7}$$

Next, we introduce a special form of graph operation: node contraction, which merges two different nodes while preserving the number of links [10]. If a graph h can be obtained by any number of node contraction operations on another graph g, we will call h a child graph of g, and g a parent graph of h. For example, in Fig. 1, graph a is a parent graph of c, and graph b is also a parent graph of c, but there is no parent-child relationship between a and b. Note that $[g]$ represents the total number of unique subgraphs of type g and of its child types on the given graph.

Then it can be shown (see **Appendix A**) that

$$Z(\beta) = M^N \exp\left\{ \sum_{\text{connected } g} \frac{(-\beta/2)^{n(g)}}{n(g)!} H(g)[g] \right\}, \quad (8)$$

where the summation is over all possible connected subgraphs g. $H(g)$ is defined as

$$H(g) = K(g)E(g) + \sum_{g' \in \mathcal{P}(g)} (-1)^{m(g,g')} K(g,g') K(g') E(g'), \quad (9)$$

where $K(g)$ is the combinatoric factor to construct graph g from $n(g)$ links, $K(g,g')$ is the combinatoric factor to generate graph g from graph g' by node contraction, $m(g,g')$ is the number of contraction operations required to construct g from g', and $\mathcal{P}(g)$ is the set containing all parent graphs of graph g. Finally, the free energy is

$$F(\beta) = -Nk_BT \ln M + \sum_{\text{connected } g} \tilde{F}(g,\beta), \quad (10)$$

where

$$\tilde{F}(g,\beta) = -\frac{1}{\beta} \frac{(-\beta/2)^{n(g)}}{n(g)!} H(g)[g]. \quad (11)$$

One advantage of equations 10 and 11 is that the graph topology (which determines $[g]$) is now unlinked from detailed energetics (which determines $H(g)$). Hence, even without knowing the exact energy matrix E, it is possible to compare $[g]$ values from different structures and, in some cases, we can determine which structure provides lower free energy of the corresponding spin system. To illustrate this, let us consider two different graph systems, a chain graph of length N and a star graph with N leaves. They have the same numbers of nodes and links, but it can be shown that $[g]^{\text{chain}} < [g]^{\text{star}}$ holds in general (see **Appendix B**), so at a temperature high enough that, for the star graph, the infinite sum in equation 10 does not diverge and if the sum is negative (stable free energy), we can conclude that the star-graph spin system has lower free energy than its counterpart on a chain graph. Note that this qualitative result is independent of the details of the energy matrix. As a specific example, an Ising chain system always has higher free energy than an Ising star at any $T > 0$ regardless of the details of energetics (see **Appendix B**).

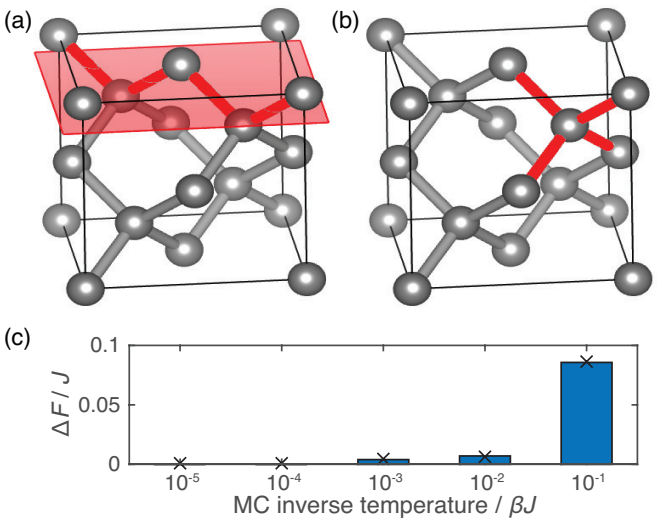

FIG. 2: (a-b) Two different types of defects, drawn by VESTA 3 [11]. Broken bonds are marked in red. (a) Diamond structure with a grain boundary indicated by a red plane. (b) Same structure with a vacancy defect. (c) Difference between MC free energies of two Si-Ge alloy lattice systems with different types of defects, as a function of inverse temperature. Here, the y axis shows $\Delta F = F(\text{vacancy defect}) - F(\text{grain boundary})$ for the entire system.

A possible application of this general analysis is to an alloy lattice system with defects. Here we consider two types of defects: planar defects (*i.e.*, grain boundaries) and point defects. We constructed a 3-dimensional diamond-like lattice structure in $3 \times 3 \times 3$ unit cells with a periodic boundary condition (216 lattice points). The first system contains a grain boundary modeled by a discontinuity on the (001) plane (see Fig. 2a). To simulate vacancy defects, we constructed a second system by removing lattice points randomly (see Fig. 2b) until the number of broken bonds was equal to the number of bonds broken at the grain boundary in the first system (the number of remaining bonds = 324). Using a similar argument as above, it can be analytically shown that $[g]$ is generally greater for the point vacancy system than for the grain boundary system.

We carried out a Monte Carlo (MC) simulation to check that the system with point vacancies indeed has lower free energy than that with a grain boundary. We considered lattice site occupation with the atom types $s(i) = \text{Si}, \text{Ge}$ as the possible states of lattice site i, and used the interatomic potential developed in previous works [12, 13]. Assuming equal bond lengths, $E(\text{Si},\text{Si}) = -2.17J, E(\text{Ge},\text{Ge}) = -1.93J, E(\text{Si},\text{Ge}) = -2.04J$, where J is a constant. We tested five different temperatures, $10^{-1}, 10^{-2}, 10^{-3}, 10^{-4}$, and 10^{-5} in units of βJ. We car-

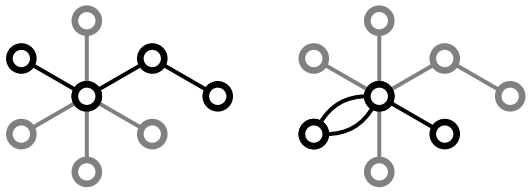

(a) (b)

FIG. 3: Examples of subgraphs (black) contributing to the term $[g]$ where g is a 3-link path graph (Fig. 1a) on the given graph architecture (gray). (b) shows a child graph of a 3-link path graph (Fig. 1c).

ried out 1,000 independent MC simulations for each temperature, and in each simulation we performed 1.1 million MC steps and neglected the first 0.1 million steps to achieve the system equilibrium (see Fig. S3 for a representative trajectory).

Fig. 2c shows the MC free energy difference between the two systems with different defect types as a function of βJ. In the high-temperature regime, the constant term and one-link term (proportional to the number of links) in equation 10 dominate so that the difference between the two systems is negligible. However, as inverse temperature βJ increases, the free energy difference between the two systems increases as well. The point defect system has lower free energy as expected, which is consistent with the experimentally known fact that point vacancies have thermal equilibrium concentrations whereas higher-dimensional defects cannot be formed spontaneously [14]. The entropic effect of multiple vacancy configurations and the stabilizing effect of structure relaxation have previously been used to explain this difference [15], but both factors were constant in our simulations so they cannot account for the free energy differences observed here. Also, the numbers of broken bonds are equal, meaning that the "surface areas" are the same. Thus, this result implies that the stability of point defects (compared to line and planar defects) is partially due to the lattice topology itself.

We have hitherto considered qualitative differences between different graphs. Can we make a quantitative prediction of the system free energy? Although it is impossible to obtain a general closed form of equation 10, a closed form can be obtained for some special types of contributing graphs. We will focus on a path subgraph [16] (see Fig. 3a). Among tractable subgraphs, this type of graph has a significant contribution, because it does not have any connected parent graph and $[g] \geq [h]$ if g is a parent graph of h, so that the path graph provides one of the largest $[g]$ values among the connected graphs with the same number of links.

For a path subgraph g of length $n(g)$,

$$[g] = \sum A_{i_0 i_1} A_{i_1 i_2} \cdots A_{i_{n(g)-1} i_{n(g)}} = \text{su } A^{n(g)}, \quad (12)$$

where su A is defined as the element sum of A, *i.e.* $\sum_{ij} A_{ij}$. Note that this term contains contributions from child subgraphs of g (see Fig. 3b). Similarly, we can express $E(g)$ for a path subgraph g by a relatively simple form,

$$E(g) = M^{-n(g)-1} \text{su } E^{n(g)}, \quad (13)$$

and we will define $\tilde{F}_{\text{path}}(\beta)$ as the summation of free energy contributors corresponding to path graphs:

$$\tilde{F}_{\text{path}}(\beta) = \sum_{\text{path } g} -\frac{1}{\beta} \frac{(-\beta/2)^{n(g)}}{n(g)!} K(g) E(g) [g]. \quad (14)$$

By using matrix diagonalization (see **Appendix C**), it can be shown that

$$\tilde{F}_{\text{path}}(\beta) = \frac{1}{2M^2} \sum_{i,j}^{N,M} \frac{|c_i|^2 |d_j|^2 \lambda_i \mu_j}{1 + \beta \lambda_i \mu_j / M}, \quad (15)$$

for $Mk_BT > \max(|\lambda_i|) \max(|\mu_j|)$. Here $\{\lambda_i\}$ and $\{\mu_j\}$ respectively represent the spectra of A and $\epsilon = E - \sum_{ij} E_{ij}/M^2$, and their corresponding eigenvector sets are respectively $\{|i\rangle_A\}$ and $\{|j\rangle_\epsilon\}$. We use inner products $c_i = \langle \mathbf{1} | i \rangle_A$ and $d_j = \langle \mathbf{1} | j \rangle_\epsilon$, by denoting an all-ones vector by $|\mathbf{1}\rangle$.

The free energy formula with the path graph factor is

$$F(\beta) = -Nk_BT \ln M + \frac{1}{2} E_0 \cdot \text{su } A - \frac{\beta}{4M^2} \left(\text{tr } \epsilon^2 - \frac{2}{M} \text{su } \epsilon^2 \right) \text{tr } A^2 + \frac{1}{2M^2} \sum_{i,j} \frac{|c_i|^2 |d_j|^2 \lambda_i \mu_j}{1 + \beta \lambda_i \mu_j / M} + \mathcal{O}(\beta^2), \quad (16)$$

where tr A indicates the trace of A, while a simple linear approximation of equation 10 (see **Appendix D**) gives

$$F(\beta) = -Nk_BT \ln M + \frac{1}{2} E_0 \cdot \text{su } A - \frac{\beta}{4M^2} \left\{ \left(\text{tr } \epsilon^2 - \frac{2}{M} \text{su } \epsilon^2 \right) \text{tr } A^2 + \frac{2}{M} \text{su } \epsilon^2 \text{su } A^2 \right\} + \mathcal{O}(\beta^2). \quad (17)$$

To illustrate the utility of those approximate formulae, let us consider an example from biophysics. The des-

ignability of a protein structure is defined as the number of sequences that fold into the given structure as their lowest energy state. Biophysicists have been used this concept to investigate the principles of protein design and protein evolution (for review, see [17]). As previously discussed [18], there is a strong relationship between designability and sequence space free energy, *i.e.* the free energy of a heteropolymer in sequence space, instead of conformation space.

The Hamiltonian of a protein structure is given by

$$\mathcal{H} = \frac{1}{2}\sum_{i,j}^{N,N} A_{ij} E_{\mathrm{AA}(i)\mathrm{AA}(j)}. \tag{18}$$

Here A is called a contact matrix in the protein structure literature. Each element of A, A_{ij}, is 1 when residues i and j are nearest neighbors on the lattice but not adjacent on the protein backbone, and $A_{ij} = 0$ otherwise. E is an interaction matrix that contains interaction energies for every pair of amino acid types. N is the chain length, and $\mathrm{AA}(k)$ is the amino acid type of residue k. This formula is analogous to the Hamiltonain for a spin model (equation 1; see [19]), so we can apply equation 16, or equation 17 to calculate the sequence space free energy at high sequence space temperature (where mutations can occur relatively frequently).

We studied the sequence space of a 3×3×3 lattice protein structure (Fig. 4, upper left), whose intra-chain interaction network can be represented by a graph with 27 nodes and 28 links (the total number of non-covalent contacts). We used 10,000 representative structures among 103,346 maximally compact structures [20] to reduce the computational cost, following Heo *et al* [21]. We also employed two types of amino acids, and the interaction matrix represents hydrophobic and polar interactions:

$$E = \begin{bmatrix} -3J & J \\ J & 0 \end{bmatrix} \tag{19}$$

We designated an arbitrary chosen conformation as "native structure" and scanned all 2^{27} (about 1.3×10^8) possible sequences to compute $Z(\beta) = \sum_{\text{sequences}} e^{-\beta\mathcal{H}}$ and the corresponding $F(\beta)$ for a given β. We denote this F as the "exact sequence space free energy," to distinguish it from a prediction made using equation 16 or 17, which we will call the "predicted sequence space free energy." We repeated this calculation for all 10,000 structures.

Fig. 4 shows the sequence space free energy distributions over 10,000 lattice proteins at temperature $\beta J = 0.1$. The predicted values from equation 16 correlate strongly with the exact values (red, right axis), while predictions using the simpler approximation, equation 17, are not capable of discriminating between structures with different sequence space free energies (blue, left axis). The deficiency of equation 17 is due to degeneracies in su A^2 and tr A^2, which equation 17 cannot

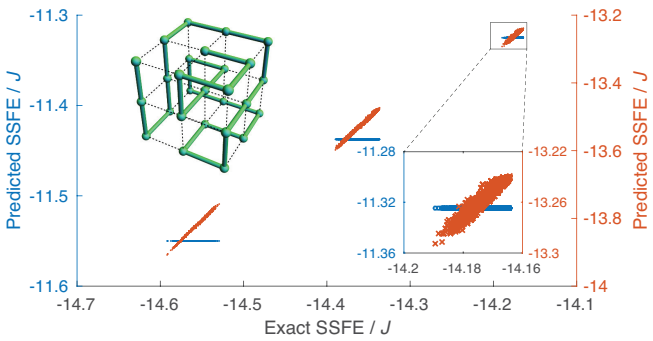

FIG. 4: Scatter plots of sequence space free energy (SSFE) distributions for 10,000 lattice protein structures, comparing exact and predicted SSFEs at $\beta J = 0.1$. Equation 16 (red) and equation 17 (blue) were used to calculate predicted SSFEs. (Upper left) a cartoon of a prototypical lattice protein. (Lower right) zoom of the boxed region.

resolve. However, even in the former case, strict one-to-one correspondence does not hold between the exact and predicted values (lower right), because of contributions from higher-order terms that $\tilde{F}_{\mathrm{path}}(\beta)$ does not capture. Note that the structures are mainly grouped by three different su A^2 values, implying that the system is still in the high-temperature regime, where higher-order terms do not dominate.

In this Letter, we presented an analytical method for calculating the free energy of a spin model on a simple graph. Through this approach, we find that the free energy contribution of the graph topology, realized by products of adjacency matrix elements, can be separated from energetic factors. The theory was illustrated by comparing chain and star graphs. Without specifying the interaction matrix, we showed that the star graphs are more stable than chain graphs in the high-temperature regime. The approach was then applied to lattice models of alloys with different defect types, which lead to different free energies, even when the systems had the same defect surface areas. We also showed that linear graphs are special in the sense that their infinite sum can be computed exactly, and this approach was applied to the protein design problem. The relative order of sequence space free energies of lattice proteins was predicted relatively accurately by the formula containing the infinite sum from the linear graph contribution, whereas a mere linear approximation could not discriminate among structures with the same su A^2 values. We hope that this theory will be expanded and applied to other graph-related problems in physics, from more complex spin systems to biological systems and also social networks.

We appreciate valuable comments from Erel Levine and Kunok Chang. This work is supported by NIH grant GM068670.

* jeongmochoi@fas.harvard.edu
† amygilson@fas.harvard.edu
‡ shakhnovich@chemistry.harvard.edu

[1] D. J. Watts and S. H. Strogatz, Nature **393**, 440 (1998).
[2] R. Albert and A.-L. Barabási, Rev. Mod. Phys. **74**, 47 (2002).
[3] R. Pastor-Satorras and A. Vespignani, *Evolution and Structure of the Internet: A Statistical Physics Approach* (Cambridge University Press, 2007).
[4] S. Dorogovtsev and J. Mendes, *Evolution of Networks: From Biological Nets to the Internet and WWW* (OUP Oxford, 2013).
[5] S. N. Dorogovtsev, A. V. Goltsev, and J. F. F. Mendes, Rev. Mod. Phys. **80**, 1275 (2008).
[6] I. Farkas, I. Derényi, G. Palla, and T. Vicsek, Lect. Notes. Phys. **650**, 163 (2004).
[7] R. Kőnig and R. Eils, Bioinformatics **20**, 1500 (2004).
[8] C. Bisconti, A. Corallo, L. Fortunato, A. A. Gentile, A. Massafra, and P. Pellè, Frontiers in Psychology **6**, 1698 (2015).
[9] A simple graph is defined as a graph with no self-loops on any node and no mulitple links between any pair of nodes. It may be either connected or disconnected.
[10] S. Hartung and N. Talmon, in *Theory and Applications of Models of Computation: 12th Annual Conference, TAMC 2015, Singapore, May 18-20, 2015, Proceedings*, Lecture Notes in Computer Science, edited by R. Jain, S. Jain, and F. Stephan (Springer International Publishing, 2015) pp. 260–271.
[11] K. Momma and F. Izumi, J. Appl. Cryst. **44**, 1272 (2011).
[12] M. Laradji, D. P. Landau, and B. Dünweg, Phys. Rev. B **51**, 4894 (1995).
[13] L. Cannavacciuolo and D. P. Landau, Phys. Rev. B **71**, 134104 (2005).
[14] L. Priester, in *Grain Boundaries: From Theory to Engineering* (Springer Netherlands, Dordrecht, 2013) Chap. 5, pp. 135–146.
[15] Y. Tateyama and T. Ohno, Phys. Rev. B **67**, 174105 (2003).
[16] A path graph is a graph where two (terminal) nodes have vertex degree 1 and the other nodes have degree 2.
[17] N. V. Dokholyan, in *Structural Bioinformatics*, edited by P. Bourne and J. Gu (John Wiley & Sons, 2009) Chap. 39, pp. 963–984.
[18] J. L. England and E. I. Shakhnovich, Phys. Rev. Lett. **90**, 218101 (2003).
[19] E. Shakhnovich and A. Gutin, Protein Eng. **6**, 793 (1993).
[20] E. Shakhnovich and A. Gutin, J. Chem. Phys. **93**, 5967 (1990).
[21] M. Heo, S. Maslov, and E. Shakhnovich, Proc. Nat. Acad. Sci. U. S. A. **108**, 4258 (2011).

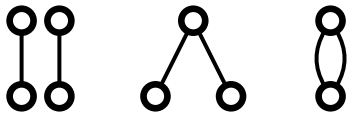

(a) (b) (c)

FIG. S1: Diagrammatical representations for three different types of two-link multigraphs.

SUPPLEMENTAL MATERIAL

Appendix A: Derivation of Equations 8 and 9

As described in the text, the Hamiltonian and partition function are respectively given by

$$\mathcal{H} = \frac{1}{2}\sum_{i,j}^{N,N} A_{ij} E_{s(i)s(j)} \tag{S1}$$

$$Z(\beta) = \sum_{\{s\}} 1 - \beta \sum_{\{s\}} \mathcal{H} + \frac{\beta^2}{2!}\sum_{\{s\}} \mathcal{H}^2 - \cdots . \tag{S2}$$

The first summation in $Z(\beta)$ is simply the number of all possible state configurations: M^N. This is a purely entropic term. Moving to the $\mathcal{O}(\beta)$ term, each link (i.e. nonzero A_{ij}) contributes an energetic contribution of $\sum_{s(i),s(j)} E_{s(i)s(j)}$, while the remaining nodes (other than i and j) contribute entropically by M^{N-2}. In other words,

$$\sum_{\{s\}} \mathcal{H} = \frac{1}{2} M^{N-2} \sum_{i,j} A_{ij} \sum_{k,l} E_{kl} \tag{S3}$$

$$= \frac{1}{2} M^{N} \sum_{i,j} A_{ij} E_0, \tag{S4}$$

where E_0 is the average energy. Noting that $\sum A_{ij}/2$ is the total number of links, equation S4 describes the mean-field energetic contribution.

Next, let us explicitly calculate the $\mathcal{O}(\beta^2)$ term in equation S2:

$$\frac{\beta^2}{2!}\sum_{\{s\}} \mathcal{H}^2 = \frac{\beta^2}{2!\cdot 4} \sum_{ijkl} A_{ij}A_{kl} \sum_{\{s\}} E_{s(i)s(j)} E_{s(k)s(l)}, \tag{S5}$$

and there are three different types of energetic contributions, depending on the relationship between the two node pairs (i,j) and (k,l). The contribution of each type is represented diagrammatically in Fig. S1, where each link represents a single energy term. Note that the graphs are no more simple in these diagrams; they are *multigraphs*, which allow multiple links.

To be particular, Fig. S1 describes three different cases: (a) the pairs are totally disconnected (no nodes are same), in which case energetic contribution is $M^{N-4}\sum_{m,n,p,q} E_{mn}E_{pq}$. (b) They share only one of their nodes ($i = k$ or $i = l$ or $j = k$ or $j = l$; other nodes are all different). The contribution is $M^{N-3}\sum_{m,n,p} E_{mn}E_{np}$. (c) The two pairs are identical (either $i = k$ and $j = l$, or $i = l$ and $j = k$). The contribution to the partition function is $M^{N-2}\sum_{m,n} E_{mn}^2$. This is where our general definition of $E(g)$ in the main text came from:

$$E(g) = M^{-n(\text{nodes})} \sum_{\text{nodes}} \prod_{k=1}^{n(g)} E_{l_k}, \tag{S6}$$

which is the energetic contribution of each multigraph normalized by the entropic contribution M^N.

The number of possible (i,j,k,l) combinations for each multigraph type should be calculated. Let us use the definition of $[g]$ in the main text:

$$[g] = \sum_{\text{nodes}} \prod_{k=1}^{n(g)} A_{l_k}, \tag{S7}$$

and the three different two-link multigraphs (Fig. S1) give

$$\left[\;\right] = \sum_{i,j,k,l} A_{ij}A_{kl} \tag{S8}$$

$$\left[\;\right] = \sum_{i,j,k} A_{ij}A_{jk} \tag{S9}$$

$$\left[\;\right] = \sum_{i,j} A_{ij}^2 \tag{S10}$$

However, they do not count the exact numbers, because equation S8 contains contributions from equations S9 and S10, and equation S9 includes those from equation S10. The exact number of contributing combinations for graph type g, which will be denoted as $W(g)$, is given as follows:

$$W\left(\;\right) = 2\left[\;\right] \tag{S11}$$

$$W\left(\;\right) = 4\left\{\left[\;\right] - W\left(\;\right)\right\} \tag{S12}$$

$$W\left(\;\right) = \left[\;\right] - W\left(\;\right) - W\left(\;\right) \tag{S13}$$

The factors of 2 and 4 respectively in equations S11 and S12 come from the symmetry counting.

Furthermore, the energy contribution can be decomposed by defining energy deviation $\epsilon_{kl} = E_{kl} - E_0$. Considering that $\sum_{k,l} \epsilon_{kl} = 0$, arithmetics leads to

$$\sum_{k,l} E_{kl}^2 = M^2 E_0^2 + \sum_{k,l} \epsilon_{kl}^2, \tag{S14}$$

$$\sum_{k,l,m} E_{kl}E_{lm} = M^3 E_0^2 + \sum_{k,l,m} \epsilon_{kl}\epsilon_{lm}, \tag{S15}$$

$$\sum_{k,l,m,n} E_{kl}E_{mn} = M^4 E_0^2. \tag{S16}$$

Therefore, the explicit form of the $\mathcal{O}(\beta^2)$ term (equation S5) is

$$\frac{\beta^2}{2!\cdot 4}\left[W\left(\right)M^{N-4}\cdot M^4E_0^2+W\left(\right)M^{N-3}\left(M^3E_0^2+\sum_{k,l,m}\epsilon_{kl}\epsilon_{lm}\right)+W\left(\right)M^{N-2}\left(M^2E_0^2+\sum_{k,l}\epsilon_{kl}^2\right)\right], \tag{S17}$$

which becomes

$$\frac{\beta^2}{2!\cdot 4}M^N\left\{E_0^2\left[W\left(\right)+W\left(\right)+W\left(\right)\right]+W\left(\right)M^{-3}\sum_{k,l,m}\epsilon_{kl}\epsilon_{lm}+W\left(\right)M^{-2}\sum_{k,l}\epsilon_{kl}^2\right\}, \tag{S18}$$

or, using equations S11, S12, and S13,

$$\frac{\beta^2}{2!\cdot 4}M^N\left\{E_0^2\left[\right]+4M^{-3}\sum_{k,l,m}\epsilon_{kl}\epsilon_{lm}\left[\right]+\left(2M^{-2}\sum_{k,l}\epsilon_{kl}^2-8M^{-3}\sum_{k,l,m}\epsilon_{kl}\epsilon_{lm}\right)\left[\right]\right\}. \tag{S19}$$

Note that the first term in parentheses is indeed

$$E_0^2\left[\right]=E_0^2(\sum A_{ij})^2=E_0^2\left[\right]^2=\left\{E_0W\left(\right)\right\}^2. \tag{S20}$$

To systematically expand this approach to higher-order terms, we will use the node contraction operation. As shown above, the critical step is calculation of $W(g)$, the exact degeneracy of graph g. Once we know $W(g)$, the partition function can be written in the form of

$$Z(\beta)=M^N\left\{1+\sum_g\frac{(-\beta/2)^{n(g)}}{n(g)!}W(g)E(g)\right\}, \tag{S21}$$

where $n(g)$ is the number of links in graph g and the summation is over all possible (connected and disconnected) graphs g. As defined in the main text, let us consider child and parent graphs: a child graph h of graph g is obtained by contraction of unconnected nodes in graph g, and g is called a parent graph of h. Note that a child graph has the same number of links as its parent. Then, generally the following equation holds:

$$W(g)=K(g)\left\{[g]+\sum_{g'\in\mathcal{C}(g)}(-1)^{m(g',g)}K(g',g)[g']\right\}, \tag{S22}$$

where $K(g)$ is the combinatoric factor to construct graph g from $n(g)$ links, $K(g',g)$ is the combinatoric factor to generate graph g' from graph g by node contraction, $m(g',g)$ is the minimal number of contraction operations required to construct g' from g, and $\mathcal{C}(g)$ is the set containing all child graphs of graph g. Since the number of links is same for parent and child graphs, we can write equation S21 in terms of $[g]$ by using the following formula: for the given number of links n,

$$\sum_{\substack{g\ s.t.\\ n(g)=n}}W(g)E(g)=\sum_{\substack{g\ s.t.\\ n(g)=n}}H(g)[g], \tag{S23}$$

where

$$H(g)=K(g)E(g)+\sum_{g'\in\mathcal{P}(g)}(-1)^{m(g,g')}K(g,g')K(g')E(g') \tag{S24}$$

and $\mathcal{P}(g)$ is a set containing all parents of graph g. This is equation 9 in the main text, and we can convert equation S21 into equation 8 in the main text:

$$Z(\beta)=M^N\left\{1+\sum_g\frac{(-\beta/2)^{n(g)}}{n(g)!}H(g)[g]\right\}, \tag{S25}$$

Note that since

$$K(g)+\sum_{g'}(-1)^{m(g,g')}K(g,g')K(g')=0 \tag{S26}$$

unless g is a one-node graph, we can always replace $E(g)$ in equation S24 by $\epsilon(g)$, which is defined as

$$\epsilon(g)=M^{-n(\text{nodes})}\sum_{\text{nodes}}\prod_{k=1}^{n(g)}(E_{l_k}-E_0), \tag{S27}$$

which will be used in **Appendix C**.

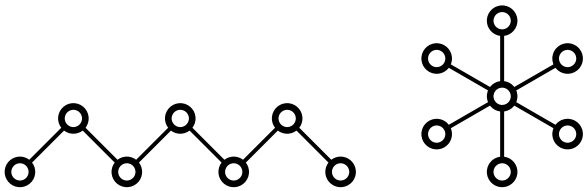

(a) (b)

FIG. S2: The 6-link chain and star graphs.

Appendix B: The Chain and Star Graph Systems

In the main text, we introduced the chain and star graphs (Fig. S2). We will show that $[g]^{\rm chain} < [g]^{\rm star}$ in general, and also investigate the Ising models on both graphs.

The elements of their adjacency matrices for the chain and star graph systems, denoted as $A^{\rm chain}$ and $A^{\rm star}$ respectively, are given below:

$$A^{\rm chain}_{ij} = \delta_{i,j+1} + \delta_{i,j-1} \tag{S28}$$

$$A^{\rm star}_{ij} = \delta_{i,1} + \delta_{j,1} - 2\delta_{i,1}\delta_{j,1}, \tag{S29}$$

where node index 1 for the star graph indicates the center node. In calculating $[g]$ for a multiple graph g, we have a summation over various products of A_{ij}, and when there is a common index (*e.g.* j in $A_{ij}A_{jk}$), the star graph gives a larger contribution to $[g]$ than the chain graph, since the two indices are disentangled in the former system. For example, let us calculate $S = \sum_{ijk} A_{ij}A_{jk}$ for both cases:

$$\begin{aligned} S^{\rm chain} &= \sum_{ijk}^{N} (\delta_{i-1,j} + \delta_{i+1,j})(\delta_{j,k+1} + \delta_{j,k-1}) \\ &= \sum_{i,k} (\delta_{i-1,k+1} + \delta_{i-1,k-1} + \delta_{i+1,k+1} + \delta_{i+1,k-1}) \\ &= (N-2) + (N-1) + (N-1) + (N-2) \\ &= 4N - 6, \end{aligned} \tag{S30}$$

where k values in $(N-k)$ terms are obtained by considering the boundary conditions. Also,

$$\begin{aligned} S^{\rm star} &= \sum_{ijk}^{N} (\delta_{i,1} + \delta_{j,1} - 2\delta_{i,1}\delta_{j,1})(\delta_{j,1} + \delta_{k,1} - 2\delta_{j,1}\delta_{k,1}) \\ &= \sum_{ijk} (\delta_{i,1}\delta_{j,1} + \delta_{i,1}\delta_{k,1} + \delta^2_{j,1} + \delta_{j,1}\delta_{k,1} + \mathcal{O}(\delta^3)) \\ &= N^2 + 3N - 4N \\ &= N^2 - N. \end{aligned} \tag{S31}$$

Here, since $\delta^2_{ij} = \delta_{ij}$, we get a quadratic dependence on N, which does not appear in the first case. Hence, $S^{\rm chain} < S^{\rm star}$ for $N > 3$. We can use a similar argument to show that

$$[g]^{\rm chain} < [g]^{\rm star}, \tag{S32}$$

in general.

The Ising model can be applied to these two graph systems. Let the energy matrix be

$$\beta E = \begin{pmatrix} -J & J \\ J & -J \end{pmatrix}, \tag{S33}$$

where $J > 0$. The partition function for the Ising chain (with open boundary conditions) is well known: for the chain length $N \geq 2$,

$$Z^{\rm chain} = 2(2\cosh J)^{N-1}. \tag{S34}$$

For the "Ising star," calculation of the partition function is straightforward:

$$Z^{\rm star} = \sum_{\{s_i\}} e^{J\sum_{\langle i,j\rangle} s_i s_j} \tag{S35}$$

$$= \sum_{\{s_i\}} e^{J\sum_{i\neq 1} s_1 s_i} \tag{S36}$$

$$= \sum_{s_1=\pm 1} \prod_{i\neq 1} \sum_{s_i=\pm 1} e^{J s_1 s_i} \tag{S37}$$

$$= (4\cosh J)^{N-1}. \tag{S38}$$

Hence, for $N = 2$, the two systems have the same free energy (and same graph structure), but for $N > 2$, $Z^{\rm chain} < Z^{\rm star}$ so that the Ising star is more stable than the Ising chain at any temperature.

Appendix C: Derivation of Equation 15

In the main text, we define

$$\tilde{F}_{\rm path}(\beta) = \sum_{\text{linear } g} -\frac{1}{\beta}\frac{(-\beta/2)^{n(g)}}{n(g)!} K(g)E(g)[g], \tag{S39}$$

and show

$$[g] = \text{su } A^{n(g)}, \tag{S40}$$

$$E(g) = M^{-n(g)-1}\text{su } E^{n(g)}, \tag{S41}$$

where su $A \equiv \sum_{ij} A_{ij}$. Also,

$$K(g) = 2^{n(g)-1} \cdot n(g)!, \tag{S42}$$

where $2^n \cdot n!$ is a combinatoric factor and due to symmetry we have the double-counting correction of $1/2$. Therefore, substitution leads to

$$\tilde{F}_{\rm path}(\beta) = -\frac{1}{2\beta M} \sum_{\substack{\text{path } g \\ s.t.\ n(g)\geq 2}} \left(-\frac{\beta}{M}\right)^{n(g)} \text{su } E^{n(g)} \text{su } A^{n(g)}. \tag{S43}$$

As shown at the end of **Appendix A**, we can rewrite the previous equation by

$$\tilde{F}_{\rm path}(\beta) = -\frac{1}{2\beta M} \sum_{\substack{\text{path } g \\ s.t.\ n(g)\geq 2}} \left(-\frac{\beta}{M}\right)^{n(g)} \text{su } \epsilon^{n(g)} \text{su } A^{n(g)}, \tag{S44}$$

where $\epsilon = E - E_0 I$.

Diagonalization helps to get a closed form of equation S44. For eigenvalues $\lambda_1 \geq \lambda_2 \geq \cdots \geq \lambda_N$ of square matrix B of size N, we have su $B^k = \sum_{i=1}^{N} |a_i|^2 \lambda_i^k$, where a_i is the inner product of the eigenvector corresponding to eigenvalue λ_i and an all-ones vector of size N. Using this, we can write

$$\text{su } A^k = \sum_{i=1}^{N} |c_i|^2 \lambda_i^k \tag{S45}$$

$$\text{su } \epsilon^k = \sum_{j=1}^{M} |d_j|^2 \mu_j^k. \tag{S46}$$

where $\{\lambda_i\}$ and $\{\mu_i\}$ represent the spectra of A and ϵ respectively, and $\{c_i\}$ and $\{d_i\}$ correspond to $\{a_i\}$ above for A and ϵ respectively. Thus, equation S44 becomes

$$\tilde{F}_{\text{path}}(\beta) = \frac{1}{2M^2} \sum_{i,j}^{N,M} \frac{|c_i|^2 |d_j|^2 \lambda_i \mu_j}{1 + \beta \lambda_i \mu_j / M}, \tag{S47}$$

for $M k_B T > \max(|\lambda_i|) \max(|\mu_j|)$.

Appendix D: Derivation of Equation 17

As discussed in the main text, the free energy is given by

$$F(\beta) = -N k_B T \ln M + \sum_{\text{connected } g} \tilde{F}(g, \beta), \tag{S48}$$

where

$$\tilde{F}(g, \beta) = -\frac{1}{\beta} \frac{(-\beta/2)^{n(g)}}{n(g)!} H(g)[g]. \tag{S49}$$

Equation 17 is obtained by termination of the series at the linear order $\mathcal{O}(\beta)$, *i.e.*, considering only the terms with $n(g) \leq 2$:

$$F_{\text{approx}}(\beta) = -N k_B T \ln M + \sum_{\substack{\text{connected } g \\ s.t.\ n(g) \leq 2}} \tilde{F}(g, \beta), \tag{S50}$$

where, using equation S23,

$$\tilde{F}(g, \beta) = -\frac{1}{\beta} \frac{(-\beta/2)^{n(g)}}{n(g)!} W(g) E(g). \tag{S51}$$

For a one-link graph, we have

$$W\left(\text{ }\right) = \left[\text{}\right] = \sum_{ij} A_{ij}, \tag{S52}$$

and

$$E\left(\text{}\right) = H\left(\text{}\right) = \sum_{kl} E_{kl} = E_0. \tag{S53}$$

Plugging these and equations S11 and S12 into equation S50, we get equation 17 in the main text.

Appendix E: Monte Carlo Trajectories

Figure S3 shows a set of trajectories of MC energy and a correlation function to the initial configuration, for a system with $\beta J = 0.1$. As the correlation function trajectory suggests, the system gets equilibrated relatively quickly, implying that the system temperature is comparably high. This is consistent with the assumption throughout this Letter.

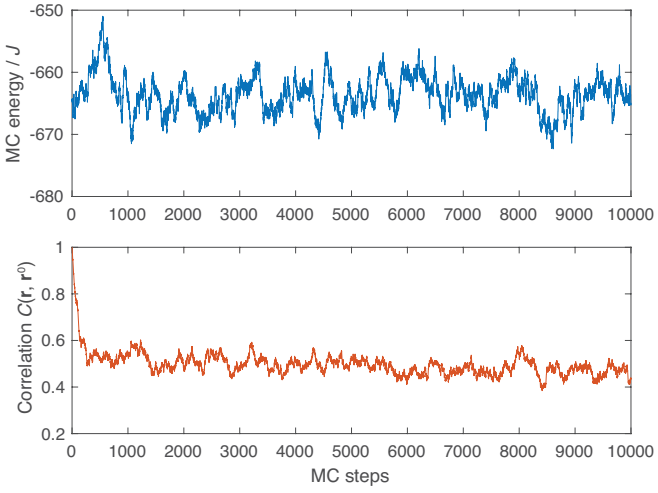

FIG. S3: Trajectory plots of MC energy (top) and a correlation function (bottom) to the initial configuration, for a system with $\beta J = 0.1$.